ELSEVIER

Journal of Nuclear Materials 255 (1998) 189–209

journal of nuclear materials

Grain boundary segregation under neutron irradiation in dilute alloys

R.G. Faulkner [a,*], Shenhua Song [a], P.E.J. Flewitt [b], M. Victoria [c], P. Marmy [c]

[a] *Institute of Polymer Technology and Materials Engineering, Loughborough University, Loughborough, Leicestershire LE11 3TU, UK*
[b] *Berkeley Centre, Magnox Electric, Berkeley, Gloucestershire GL13 9PB, UK*
[c] *EPFL-CRPP, Fusion Technology, CH-5232 Villigen PSI, Switzerland*

Received 18 June 1997; accepted 26 January 1998

Abstract

Irradiation-induced segregation mechanisms are classified into solute–point-defect complex type and inverse Kirkendall type. For solutes that have a strong interaction with interstitials in a dilute alloy, the complex effect plays an important part in the segregation. Our earlier model describing solute grain boundary segregation during neutron irradiation in dilute binary alloys, based on the complex effect mechanism, is modified by considering the irradiation-enhanced solute diffusion and the long-range recombination effect of freely migrating point-defects, and expanded to evaluate solute segregation in dilute ternary alloys through consideration of solute–solute competition for segregation sites. Applications of the model to predictions of P grain boundary segregation in neutron irradiated α-Fe and Fe–B–P and Fe–C–P alloys indicate that the model has reasonable validity.

1. Introduction

Irradiation-induced segregation mechanisms can be described by inverse Kirkendall models or solute–point-defect complex models [1–3]. The Kirkendall effects are based on the concept that components in a diffusion couple diffuse via vacancies at different rates so that a composition gradient may induce a net flux of vacancies across a lattice plane, even if the vacancy distribution is initially uniform. During neutron irradiation, the inverse situation exists near sinks such as grain boundaries and free surfaces where gradients in the vacancy and interstitial concentrations may result in a net flux of solute and solvent atoms across the lattice plane. In multicomponent systems, relative diffusion rates of various components determine their enrichment or depletion at the sinks.

If a solute has a strong interaction with point-defects, the solute–point-defect complex effects need to be taken into consideration. The complex effects are based on the following considerations. Solute atoms, point-defects, and their complexes are in equilibrium with each other at a given temperature. Neutron irradiation produces cascades of point-defects, leading to the formation of Frenkel pairs, and as a result the point-defect concentration exceeds the thermal equilibrium concentration in the matrix. However, at sinks such as grain boundaries and free surfaces the point-defect concentration approaches the thermal equilibrium concentration. This decrease in point-defect concentration results in the dissociation of the complexes, which, in turn, leads to a decrease in the concentration of the complexes and an increase in the concentration

* Corresponding author.

0022-3115/98/$19.00
PII: S0022-3115(98)00022-1

of individual solute atoms in the proximity of sinks. In regions away from the sinks, the steady state concentration of the complexes remains, giving rise to a complex concentration gradient between the sink and the adjacent matrix. The concentration gradient of complexes causes their migration leading to an excess solute concentration in the vicinity of sinks. It is evident that the larger the supersaturation level of point-defects induced by neutron irradiation, the larger is the potential segregation of solute atoms to the sinks.

In general, the contribution of solute–point-defect complexes to solute segregation depends on their binding and migration energies. The complex mechanism during irradiation is expected to be especially important to solute migration in dilute alloys by means of interstitial–solute complexes [1,4]. This is because [4–7] (1) the migration of solute–interstitial complexes is easier than that of solute–vacancy complexes and (2) the interaction of the undersized solute with the interstitial is much stronger than that with the vacancy. As a consequence, it is clear that, for solutes which have strong interactions with interstitials, for example, phosphorus and silicon in steels and nickel alloys, the diffusion of solute–interstitial complexes should be dominant in neutron irradiation-induced segregation. However, as discussed in Ref. [1], in the absence of solute–interstitial interactions, solute segregation to sinks may occur via solute–vacancy complexes if the solute–vacancy binding energy is high enough even though the migration of solute–vacancy complexes is quite slow as compared to that of solute–interstitial complexes. Therefore, in order to clearly demonstrate whether the solute–interstitial complex effects or the solute–vacancy complex effects dominate during neutron irradiation-induced segregation, it is necessary to make predictions assuming the presence of each defect type separately.

Recently, we [3] have developed a model describing solute segregation under neutron irradiation in dilute binary alloys on the basis of the complex mechanism. In the model, both irradiation-enhanced solute diffusion and solute–interstitial complex effects are considered. To determine whether the solute–interstitial or solute–vacancy complexes play a dominant role in neutron irradiation-induced segregation, predictions of phosphorus grain boundary segregation in neutron irradiated α-Fe have been made by means of our model [3] with modifications to include the irradiation-enhanced solute diffusion theory and the long-range recombination effect of freely migrating vacancies and interstitials generated from the cascades. Predictions have also been made of solute segregation in dilute ternary Fe–B–P and Fe–C–P alloys through consideration of solute–solute competition for segregation sites on the grain boundary.

2. Theoretical models

In this section, we develop various non-equilibrium and equilibrium segregation models that are appropriate to solute or impurity segregation in simple binary alloys and more complex ternary alloys. In the latter, the issue of site competition is addressed. Moreover, we consider the input parameters that are required to support the modelling.

2.1. Irradiation-induced non-equilibrium segregation

An irradiation-induced grain boundary segregation model established in our previous work [3] is utilised to describe the process. The model originally predicted the maximum amount of segregation expected in a dilute binary alloy on the basis of a thermodynamic argument using the equilibrium concentration of point-defects expected at grain boundaries ratioed to the non-equilibrium concentration expected within grains induced during neutron irradiation. The maximum concentration of irradiation-induced non-equilibrium segregation of solute or impurity atoms, $C_{\mathrm{br}}^{\mathrm{m}}$, is given by [3]

$$C_{\mathrm{br}}^{\mathrm{m}} = C_{\mathrm{g}} \frac{E_{\mathrm{b}}^{\mathrm{ip}}}{E_{\mathrm{f}}^{\mathrm{p}}} \left[1 + \frac{BG}{A_{\mathrm{p}} D_{\mathrm{p}} k_{\mathrm{dp}}^2} \exp\left(\frac{E_{\mathrm{f}}^{\mathrm{p}}}{kT} \right) \right], \tag{1}$$

where C_{g} is the solute concentration in the matrix; p stands for the point-defect, either the vacancy, v, or the interstitial I; D_{p} is the diffusion coefficient of point-defects in the matrix; $E_{\mathrm{b}}^{\mathrm{ip}}$ is the solute–point-defect binding energy; $E_{\mathrm{f}}^{\mathrm{p}}$ is the point-defect formation energy; A_{p} is a constant associated with the vibrational entropy of atoms around the point-defect; G is the point-defect production rate (or neutron dose rate); k is Boltzmann's constant; T is the absolute temperature; B is the dose rate correction factor, i.e., the fraction of freely migrating point-defects escaping from the cascade; and k_{dp}^2 is the sink strength for point-defects. There are two sink strengths, one of which, k_{dI}^2, is for interstitials and the other, k_{dv}^2, for vacancies, and they are given by [2]

$$k_{\mathrm{dI}}^2 = \sqrt{Z_{\mathrm{I}}\rho} \left(\frac{6}{R} + \sqrt{Z_{\mathrm{I}}\rho} \right) \tag{2a}$$

and

$$k_{\mathrm{dv}}^2 = \sqrt{\rho}\left(\frac{6}{R} + \sqrt{\rho}\right), \tag{2b}$$

where Z_{I} is the bias parameter defining the preferential interaction between interstitials and dislocations compared with that between vacancies and dislocations; R is the grain size; and ρ is the dislocation density, given by [3]

$$\rho = \rho_{\mathrm{o}} \exp\left(\frac{E_{\mathrm{d}}}{kT}\right) \tag{3}$$

where ρ_{o} is the dislocation density constant which depends on the pre-irradiation dislocation density, the dose rate, etc., and E_{d} is the activation energy for dislocation recovery processes.

It is evident that the maximum grain boundary segregation concentration, $C_{\mathrm{br}}^{\mathrm{m}}$, given by Eq. (1) is mainly dependent on the irradiation temperature and is independent of the irradiation time. In this important thermodynamic relationship, the effective dose rate term does not take account of long-range recombination of point-defects. As one improvement on our previous model [3], we now use the following method to evaluate the long-range recombination effects of freely migrating vacancies and interstitials outside the cascade.

During steady-state irradiation, the defect production rate, G, is described by the following equations [8]:

$$BG = \lambda C_{\mathrm{v}}^{\mathrm{r}} C_{\mathrm{I}}^{\mathrm{r}} + k_{\mathrm{dv}}^2 D_{\mathrm{v}} C_{\mathrm{v}}^{\mathrm{r}} \tag{4a}$$

$$BG = \lambda C_{\mathrm{v}}^{\mathrm{r}} C_{\mathrm{I}}^{\mathrm{r}} + k_{\mathrm{dI}}^2 D_{\mathrm{I}} C_{\mathrm{I}}^{\mathrm{r}} \tag{4b}$$

where B is the dose rate correction factor; λ is the long-range recombination coefficient of freely migrating point-defects outside the cascade; $C_{\mathrm{I}}^{\mathrm{r}}$ and $C_{\mathrm{v}}^{\mathrm{r}}$ are the irradiation-generated interstitial and vacancy concentrations, respectively; D_{I} and D_{v} are the diffusion coefficients of interstitials and vacancies, respectively. From Eqs. (4a) and (4b), one may obtain the concentration of irradiation-created point-defects (vacancies or interstitials), $C_{\mathrm{p}}^{\mathrm{r}}$, as

$$C_{\mathrm{p}}^{\mathrm{r}} = \frac{BGF(\eta)}{D_{\mathrm{p}} k_{\mathrm{dp}}^2} \tag{5}$$

where

$$F(\eta) = \frac{2}{\eta}\left[(1+\eta)^{1/2} - 1\right] \tag{6}$$

and

$$\eta = \frac{4\lambda BG}{k_{\mathrm{dv}}^2 k_{\mathrm{dI}}^2 D_{\mathrm{v}} D_{\mathrm{I}}} \tag{7}$$

where the long-range recombination coefficient of freely migrating point-defects, λ, is given by [9]

$$\lambda = \frac{21 D_{\mathrm{I}}}{b^2} \tag{8}$$

where b is the jump distance of interstitials.

With provision for the long-range recombination of freely migrating point-defects, Eq. (1) can be changed into

$$C_{\mathrm{br}}^{\mathrm{m}} = C_{\mathrm{g}} \frac{E_{\mathrm{b}}^{\mathrm{ip}}}{E_{\mathrm{f}}^{\mathrm{p}}}\left[1 + \frac{BGF(\eta)}{A_{\mathrm{p}} D_{\mathrm{p}} k_{\mathrm{dp}}^2} \exp\left(\frac{E_{\mathrm{f}}^{\mathrm{p}}}{kT}\right)\right] \tag{9}$$

As the thickness of the boundary region is very small as compared with the grain size, in which the concentration gradient may be neglected, the diffusion of the complexes towards the grain boundary may be simplified into a steady linear flow of the complexes into the grain boundary in a semi-infinite medium. One may envisage, for convenience, an interface between grain boundary and interior located exactly at $x = 0$ where the solute concentration, C, is $C = C_{\mathrm{br}}(t)/\alpha$ where $C_{\mathrm{br}}(t)$ is the solute concentration at the concentrated layer when irradiation time is equal to t, and changes with irradiation time at a given

irradiation temperature, and $\alpha = C_{br}^{m}/C_g$. In terms of the Fick's law and the Principle of Mass Conservation, the kinetics of irradiation-induced segregation may be obtained as [3]

$$\frac{C_{br}(t) - C_g}{C_{br}^{m} - C_g} = 1 - \exp\left(\frac{4D_c^{iP}t}{\alpha_n^2 d^2}\right) erfc\left(\frac{2\sqrt{D_c^{iP}t}}{\alpha_n d}\right) \tag{10}$$

where $C_{br}(t)$ is the boundary concentration of the solute at irradiation time $= t$, C_g is the solute concentration in the matrix, D_c^{iP} is the diffusion coefficient of solute–point-defect (vacancy, v, or interstitial, I) complexes, d is the boundary thickness, and α_n is the maximum non-equilibrium enrichment ratio, given by $\alpha_n = C_{br}^{m}/C_g$.

Eq. (10) is an isothermal kinetic relationship for irradiation-induced grain boundary segregation. It describes the grain boundary segregation level as a function of irradiation time at a given irradiation temperature.

The above model is only suitable for dilute binary alloys. We now expand this model to predict the irradiation-induced non-equilibrium segregation of solute atoms in dilute ternary alloys through consideration of solute–solute competition for segregation sites.

Solutes 1 and 2 in a dilute ternary alloy are here assumed to compete with each other for segregation sites at the grain boundary. The site competition between these two solutes will be dealt with by the following method. By the complex mechanism described above the solutes first segregate to the grain boundary independently to obtain segregation levels C_{br}^{S1} and C_{br}^{S2}, and then re-distribute there in proportion to their binding energies with the grain boundary (equilibrium segregation energies). The competition effect may be evaluated by

$$C_{br}^{S1*} = C_{br}^{S1}\left[\frac{C_g^{S1}\exp\left(\frac{Q_{S1}}{kT}\right)}{C_g^{S1}\exp\left(\frac{Q_{S1}}{kT}\right) + C_g^{S2}\exp\left(\frac{Q_{S2}}{kT}\right)}\right] \tag{11a}$$

$$C_{br}^{S2*} = C_{br}^{S2}\left[\frac{C_g^{S2}\exp\left(\frac{Q_{S2}}{kT}\right)}{C_g^{S1}\exp\left(\frac{Q_{S1}}{kT}\right) + C_g^{S2}\exp\left(\frac{Q_{S2}}{kT}\right)}\right] \tag{11b}$$

where C_{br}^{S1*} and C_{br}^{S2*} are the final levels of irradiation-induced grain boundary segregation for solutes 1 and 2, respectively; Q_{S1} and Q_{S2} are the binding energies of the grain boundary with solutes 1 and 2, respectively; and C_g^{S1} and C_g^{S2} are the matrix concentrations of solutes 1 and 2, respectively.

The above approach to describing the site competition between two solutes in ternary systems might be acceptable. Since irradiation-induced non-equilibrium segregation is a kinetic process, the complexes leading to this segregation may diffuse independently to the grain boundary. In a manner similar to equilibrium segregation, the two solutes, however, need to re-distribute at the grain boundary in the light of their binding energies with the boundary. Of course, interference among the complexes is likely to exist but at present this effect is difficult to evaluate.

Eq. (9) evaluating the maximum concentration of non-equilibrium segregation in binary alloys is used here to depict the maximum concentration in ternary alloys through the following considerations. As stated in Ref. [2], the absolute concentration of the complexes is proportional to the solute concentration and the exponential term containing the solute–point-defect binding energy. As a result, in order to evaluate the effect of site competition between two solutes on the maximum concentration of irradiation-induced non-equilibrium segregation, the modified absolute concentrations of complexes in the ternary situation may be included. Eq. (9) may thus be modified into

$$C_{br(Sj)}^{m} = C_g^{Sj}\frac{E_{b(Sj)}^{ip}}{E_f^{p}}\left[\frac{C_g^{Sj}\exp\left(\frac{E_{b(Sj)}^{ip}}{kT}\right)}{\sum_j C_g^{Sj}\exp\left(\frac{E_{b(Sj)}^{ip}}{kT}\right)}\right]\left[1 + \frac{BGF(\eta)}{A_p D_p k_{dp}^2}\exp\left(\frac{E_f^{p}}{kT}\right)\right], \qquad j = 1,2 \tag{12}$$

where $C_{br(Sj)}^{m}$ is the maximum concentration of irradiation-induced non-equilibrium segregation for solute j, $E_{b(Sj)}^{ip}$ is the solute j-point-defect binding energy, and C_g^{Sj} is the matrix concentration of solute j.

The kinetics for irradiation-induced grain boundary segregation are given by [3]

$$\frac{C_{br}^{Sj}(t) - C_g^{Sj}}{C_{br(Sj)}^{m} - C_g^{Sj}} = 1 - \exp\left(\frac{4D_{c(Sj)}^{ip}t}{\alpha_{n(Sj)}^2 d^2}\right) erfc\left(\frac{2\sqrt{D_{c(Sj)}^{ip}t}}{\alpha_{n(Sj)}d}\right) \qquad j = 1,2 \tag{13}$$

where $C_{br}^{Sj}(t)$ is the concentration of solute j at the concentrated layer as a function of irradiation time at a given irradiation temperature, $D_{c(Sj)}^{ip}$ is the diffusion coefficient of solute j-point-defect complexes, d is the thickness of the concentrated layer, and $\alpha_{n(Sj)} = C_{br(Sj)}^{m}/C_{g}^{Sj}$.

The time required for reaching the steady-state segregation during irradiation may be determined by a critical time approach. At this critical time the net supply of solute atoms from the grain centres becomes exhausted. After this the reverse flow of solute atoms created by the non-equilibrium segregation concentration gradient is equal to the forward flow of the complexes. This concept has been used by Martin [10] to derive the steady-state analytical solution of the Johnson–Lam rate theory model [11]. Details on the critical time may be seen in Ref. [12]. The critical time, t_c, is expressed as [2,3,12,13]

$$t_c = \frac{\delta R^2 \ln\left(\frac{D_c^{ip}}{D_i}\right)}{4\left(D_c^{ip} - D_i\right)}, \tag{14}$$

where δ is a numerical constant (quoted by Faulkner [12] as 0.05), R is the grain size, D_i is the diffusion coefficient of solute atoms in the matrix. D_i is taken to be the irradiation-enhanced diffusion coefficient D_i* for substitutional solutes or the thermal diffusion coefficient D_i^T for interstitial solutes.

It may be seen from Eq. (14) that if $D_c^{ip} < D_i$, e.g., carbon in α-Fe, there will be no non-equilibrium segregation effects. It should, however, be noted here that Eq. (14) is applicable only at higher temperatures, i.e., when the maximum equilibrium segregation level is zero or at least very low. In practice, irradiation temperatures are usually lower than 600°C. In this scenario, there is quite a high maximum equilibrium segregation level for alloying or impurity elements such as carbon, boron and phosphorus in steels. During irradiation, there will be no net back-diffusion fluxes of solute atoms from the grain boundary to the grain from which the solute atoms were transported until the maximum equilibrium segregation level is reached. In other words, the solute atoms will stick to the grain boundary even though they should be moving away from it. As a consequence, even if $D_c^{ip} < D_i$ there will still be non-equilibrium segregation effects before the maximum equilibrium segregation level is attained. This situation will be considered in the calculations, i.e., the non-equilibrium segregation will be calculated until the maximum equilibrium segregation level is reached when $D_c^{ip} < D_i$.

In general, solute diffusion in a dilute alloy may be enhanced mainly by irradiation-created vacancies and little by irradiation-created solute–interstitials. This is because the solute concentration in the dilute alloy is quite low and thus the concentration of irradiation-created solute–interstitials is quite low as well and consequently the solute diffusion is little affected by these solute–interstitials. In our previous work [3], we have described an approach to evaluating irradiation-enhanced solute diffusion. A new approach that has a clearer physical basis has been developed here.

For diffusion of substitutional solute atoms in a crystal matrix, the diffusion coefficient, D_i, can be given by [14]

$$D_i = \theta \omega p_v \tag{15}$$

where θ is a material constant, ω is the probability that a solute atom jumps into a vacant nearest-neighbour lattice site, and p_v is the probability that any given nearest-neighbour lattice site is vacant. The p_v is approximately equal to the vacancy concentration C_v (fraction of vacant lattice sites).

The ω may be obtained by

$$\omega = \nu \exp\left(-\frac{G_m}{kT}\right), \tag{16}$$

where ν is the vibrational frequency of the solute atom and G_m is the free energy required for a solute atom to migrate from a equilibrium position to another nearest one. G_m is a function of temperature. As a consequence, Eq. (15) can be rewritten into

$$\begin{aligned} D_i &= \theta \nu C_v \exp\left(-\frac{G_m}{kT}\right) \\ &= \delta(T) C_v, \end{aligned} \tag{17}$$

where $\delta(T) = \theta\nu \exp(-(G_m)/(kT))$.Under irradiation, the vacancy concentration, C_v, is given by

$$C_v = C_v^e + C_v^r. \tag{18}$$

As a result, Eq. (17) can be rewritten into

$$D_i^* = \delta(T)\left(C_v^e + C_v^r\right), \tag{19}$$

where D_i^* is the irradiation-enhanced solute diffusion coefficient.

In the absence of irradiation, D_i^* is equal to the thermal diffusion coefficient D_i^T. Consequently, $\delta(T)$ is given by

$$\delta(T) = D_i^T / C_v^e. \tag{20}$$

Thus the irradiation-enhanced solute diffusion coefficient, D_i^*, can be acquired by

$$D_i^* = D_i^T \left(\frac{C_v^e + C_v^r}{C_v^g} \right). \tag{21}$$

The irradiation-generated vacancy concentration, C_v^r, is given by Eq. (5) and the thermal equilibrium vacancy concentration, C_v^e, is given by

$$C_v^e = A_v \exp\left(- \frac{E_f^v}{kT} \right), \tag{22}$$

where A_v is a constant correlated with the vibrational entropy of atoms around the vacancy and E_f^v is the vacancy formation energy.

2.2. Equilibrium segregation

McLean [15] states that, for a solute atom with a binding energy to the lattice, Q, at any temperature, T, there will be an increased concentration of that solute on boundaries or interfaces, $C_\infty(T)$. The driving force for this is the reduction of energy, Q, of the solute on placing it in a strain-free region at the grain boundary, $C_\infty(T)$, is given by

$$C_\infty(T) = \frac{\beta C_g \exp(Q/kT)}{1 + \beta C_g \exp(Q/kT)}, \tag{23}$$

where β is a constant characterising the vibrational entropy of the grain boundary region and k is Boltzmann's constant. McLean [15] refined these ideas by accounting for time, realising correctly that the finite time is required to reach equilibrium and this is controlled by the diffusivity of solute atoms in the matrix.

The equilibrium segregation kinetics during irradiation, $C_{bq}(t)$, derived by means of Eq. (23), are given by

$$\frac{C_{bq}(t) - C_b(0)}{C_\infty(T) - C_b(0)} = 1 - \exp\left(\frac{4 D_i t}{\alpha_e^2 d^2} \right) erfc\left(\frac{2\sqrt{D_i t}}{\alpha_e d} \right), \tag{24}$$

where $C_b(0)$ is the solute concentration at the grain boundary at irradiation time = 0, i.e., the segregation level during the pre-irradiation heat-treatment of the material that was assumed in this work to be C_g unless specified and α_e is the maximum equilibrium enrichment ratio, given by $\alpha_e = C_\infty(T)/C_g$.

It should be furthermore noted here that although Eq. (10) is the same as Eq. (24) in form, they are much different in nature. Eq. (24) depicts the equilibrium grain boundary segregation induced by the solute equilibration at the boundary, whereas Eq. (10) describes the non-equilibrium grain boundary segregation induced by the complex diffusion to the boundary.

The equilibrium segregation model described above is merely suitable for dilute binary alloys. For dilute ternary alloys, the segregation model is described as follows. Two solutes 1 and 2, in a dilute ternary alloy, are considered here to compete with each other for sites at grain boundaries. The maximum equilibrium grain boundary concentrations of the two solutes in the ternary alloy at a given temperature T, $C_\infty^{S1}(T)$ and $C_\infty^{S2}(T)$, in the approximation that all possible sites at grain boundaries are available for segregation of solute atoms, are given respectively by [16]

$$C_\infty^{S1}(T) = \frac{C_g^{S1} \exp\left(\frac{Q_{S1}}{kT} \right)}{1 + C_g^{S1} \exp\left(\frac{Q_{S1}}{kT} \right) + C_g^{S2} \exp\left(\frac{Q_{S2}}{kT} \right)} \tag{25}$$

$$C_{\infty}^{S2}(T) = \frac{C_g^{S2}\exp\left(\frac{Q_{S2}}{kT}\right)}{1 + C_g^{S1}\exp\left(\frac{Q_{S1}}{kT}\right) + C_g^{S2}\exp\left(\frac{Q_{S2}}{kT}\right)}, \tag{26}$$

where C_g^{S1} and C_g^{S2} are the matrix concentrations of solutes 1 and 2, respectively; and Q_{S1} and Q_{S2} are the segregation energies of solutes 1 and 2, respectively.

The kinetics of equilibrium grain boundary segregation are given by [15]

$$\frac{C_{bq}^{Sj}(t) - C_b^{Sj}(0)}{C_{\infty}^{Sj}(T) - C_b^{Sj}(0)} = 1 - \exp\left(\frac{4D_{i(Sj)}t}{\alpha_{e(Sj)}^2 d^2}\right) erfc\left(\frac{2\sqrt{D_{i(Sj)}t}}{\alpha_{e(Sj)}d}\right) \qquad j = 1,2, \tag{27}$$

where $C_{bq}^{Sj}(t)$ is the equilibrium grain boundary segregation level of solute j after irradiation time t, $C_b^{Sj}(0)$ is the boundary concentration of solute j at irradiation time = 0, i.e., the segregation level produced during the pre-irradiation heat-treatment of the material. Similar to the binary case, this value is taken to be the matrix concentration of the solute in the calculations unless specified. $D_{i(Sj)}$ is the diffusion coefficient of solute j in the matrix ($D_{i(Sj)}$ is the irradiation-enhanced diffusion coefficient $D_{i(Sj)}*$ for substitutional solutes or the thermal diffusion coefficient $D_{i(Sj)}^{T}$ for interstitial solutes), d is the thickness of the concentrated layer, and $\alpha_{e(Sj)} = C_{\infty}^{Sj}(T)/C_g^{Sj}$.

Because of the fact that non-equilibrium segregation is a kinetic process and equilibrium segregation is a thermodynamic process, it is assumed that these two processes are independent of each other. In calculations, the total segregation level is taken to be the sum of the non-equilibrium and equilibrium segregation levels minus the matrix concentration of the solute.

2.3. Diffusion coefficients

In the preceding theoretical treatments, a number of diffusion coefficients are involved. In calculations, these diffusion coefficients are given by the following relations:

$$D_c^{iv} = D_{oc}^{iv}\exp\left(-\frac{E_m^{iv}}{kT}\right) \tag{28a}$$

$$D_c^{iI} = D_{oc}^{iI}\exp\left(-\frac{E_m^{iI}}{kT}\right) \tag{28b}$$

$$D_v = D_{ov}\exp\left(-\frac{E_m^{v}}{kT}\right) \tag{28c}$$

$$D_I = D_{oI}\exp\left(-\frac{E_m^{I}}{kT}\right) \tag{28d}$$

$$D_i^{T} = D_{oi}\exp\left(-\frac{E_i}{kT}\right) \tag{28e}$$

$$D_i^{*} = D_i^{T}\left(\frac{C_v^{e} + C_v^{r}}{C_v^{e}}\right), \tag{28f}$$

where D_c^{iI}, D_c^{iv}, D_v, D_I, and D_i^{T} are the diffusion coefficients of solute–interstitial complexes, solute–vacancy complexes, vacancies, interstitials, and solute atoms (referring to thermal solute diffusion) in the matrix, respectively; D_i* is the irradiation-enhanced solute diffusion coefficient; D_{oc}^{iv}, D_{oc}^{iI}, D_{ov}, D_{oI}, and D_{oi} are the pre-exponential constants for diffusion of solute–vacancy complexes, solute–interstitial complexes, vacancies, interstitials, and solute atoms, respectively; E_m^{iv}, E_m^{iI}, E_m^{v}, and E_m^{I} are the migration energies for diffusion of solute–vacancy complexes, solute–interstitial complexes, vacancies, and interstitials in the matrix, respectively; and E_i is the activation energy for thermal diffusion of solute atoms.

2.4. Determination of interstitial solute–interstitial binding energies

As clearly shown above, the solute–interstitial binding energy is an important parameter. We have developed an approach to evaluating this value for substitutional solute–interstitial complexes, e.g., boron or phosphorus–interstitial

complexes in α-Fe [7]. Note that boron is here thought of as a substitutional solute in α-Fe because on the basis of diffusion data [17], relative solubilities, atom diameter, and interstitial hole sizes [18] it appears that boron forms a substitutional solid solution in α-Fe and an interstitial solid solution in γ-Fe. Owing to an interstitial solute (carbon) involved in the alloys concerned in this work, we now, on the basis of the approach, consider the case of interstitial solute–interstitial complexes.

Interstitial–impurity interaction studies [4,19,20] of dilute alloys have shown that self-interstitials can be trapped by undersized substitutional solute atoms as mixed dumbbells composed of a solute atom and a matrix atom. It is assumed that the interstitials can also be trapped by interstitial solute atoms as mixed dumbbells. In this case, the solute–interstitial binding energy, E_b^{iI}, can be given by [4,7,21]

$$E_b^{iI} = E_f^I + E_f^i - E_f^{iI}, \tag{29}$$

where E_f^I, E_f^i, and E_f^{iI} are the formation energies for the self-interstitial (dumbbell), solute atom, and solute–interstitial complex (mixed dumbbell), respectively. In the calculation of the solute–interstitial binding energy, the difference between the substitutional solute–interstitial complex and the interstitial solute–interstitial complex is that they have different calculation procedures for the solute atom formation energy.

In accordance with our previous work [7], the self-interstitial formation energy, E_f^I, may approximately be given by

$$E_f^I = \frac{14\pi}{3}\mu r_k (r_o - r_k)^2 + 8\pi r_o S_o, \tag{30}$$

where r_o is the matrix atom radius, r_k is the hole radius before the dumbbell formation, S_o is the energy per unit area of the interface between a matrix and a perfect lattice, and μ is the shear modulus of the matrix. Here, S_o is assumed to be equal to the coherent twin boundary energy. The justification for this assumption may be seen in Ref. [7]. The value of the coherent twin boundary energy is about 0.019 J m^{-2} for Fe–Cr–Ni alloys. The value of r_k may approximately be given by the following relations [7].

For bcc crystals:

$$r_k = \sqrt{\frac{3a^2}{8}} - \frac{\sqrt{3a^2}}{4}. \tag{31a}$$

For fcc crystals:

$$r_k = \frac{\sqrt{5a^2}}{4} - \frac{\sqrt{2a^2}}{4}, \tag{31b}$$

where a is the lattice constant of the matrix material.

According to Chapman and Faulkner [22], the interstitial solute atom formation energy may be given by

$$E_f^i = \frac{8\pi}{3}\mu r_s (r_i - r_s)^2 + E_{sm}, \tag{32}$$

where E_{sm} is the matrix/solute interfacial energy, r_i is the solute atom radius, and r_s is the octahedral interstitial radius. The value of r_s is $0.414 r_o$ for fcc crystals. For bcc crystals, in view of the asymmetrical feature of the octahedral interstitial there are two interstitial radii R_1 ([001] orientation) and R_2 ([110] and [$\bar{1}$10] orientations), where $R_1 = 0.154 r_o$ and $R_2 = 0.633 r_o$. It is assumed here that for bcc crystals the effective value of r_s is equal to $(R_1 + 2R_2)/3$, i.e., $0.473 r_o$.

Replacing a matrix atom in the self-interstitial dumbbell by a solute atom creates an solute–interstitial complex (mixed dumbbell). The solute–interstitial complex formation energy is given by Ref. [7]:

$$E_f^{iI} = E_f^I - \frac{8\pi}{3}\mu r_k (r_o - r_k)^2 - 4\pi r_o^2 S_o + \frac{8\pi}{3}\mu r_k (r_i - r_k)^2 + E_{sm}. \tag{33}$$

Hence the interstitial solute–interstitial binding energy may be given by

$$\begin{aligned} E_b^{iI} &= E_f^I + E_f^i - E_f^{iI} \\ &= \frac{8\pi}{3}\mu\left[r_s (r_i - r_s)^2 + r_k (r_o - r_k)^2 - r_k (r_i - r_k)^2 \right] + 4\pi r_o^2 S_o \end{aligned}. \tag{34}$$

For ferritic steel matrices, a is 0.286 nm [23] and r_k is then obtained to be 0.0512 nm. Using $\mu = 8.1 \times 10^4$ MN m^{-2}, $r_o = 0.1241$ nm, and $r_{i(C)} = 0.077$ nm, one can acquire the carbon-interstitial binding energy in the ferritic steel matrix as

1.12 eV. The substitutional impurity–interstitial binding energy in the ferritic steel matrix has already been obtained as 0.57 eV for phosphorus–interstitial complexes and 1.11 eV for boron–interstitial complexes in our previous work [7].

3. Results and discussion

The newly modified model described in Section 2 is now applied to the segregation of phosphorus in α-Fe and Fe–C–P and Fe–B–P alloys subjected to neutron irradiation. In the predictions, the solute–interstitial and solute–vacancy complex effects are treated separately so as to determine whether the solute–interstitial or solute–vacancy complexes play a dominant role in neutron irradiation-induced non-equilibrium segregation. Data used in the theoretical calculations are listed in Table 1.

Fig. 1 illustrates the phosphorus diffusion coefficients in the α-Fe matrix as a function of temperature for thermal diffusion and irradiation-enhanced diffusion, at a neutron dose rate of 10^{-8} dpa s^{-1}, a grain size of 10 mm, and a dislocation density constant (ρ_o) of 10^{16} m^{-2} typical of that for quenched steels. Above $\sim$320°C, the irradiation-enhanced diffusion coefficient is the same as the thermal diffusion coefficient. This is because, above $\sim$320°C, the irradiation-created vacancy concentration is relatively small compared with the thermal equilibrium vacancy concentration. Below $\sim$320°C, there are apparent irradiation-enhanced diffusion effects.

The results for phosphorus segregation in α-Fe, predicted by the model, are illustrated in Figs. 2–6. Fig. 2 shows the temperature dependencies of equilibrium (C1) and non-equilibrium (predicted by the solute–interstitial complex (C2) and solute–vacancy complex (C3) models) phosphorus grain boundary segregation in α-Fe subjected to neutron irradiation with $\rho_o = 10^{16}$ m^{-2}, $R = 10$ μm, neutron dose rate $= 10^{-8}$ dpa s^{-1}, and neutron dose $= 1$ dpa. Clearly, the equilibrium segregation of phosphorus is dominant at higher temperatures whereas the irradiation-induced non-equilibrium segregation is dominant at lower temperatures. Fig. 2 also shows that the solute–interstitial complex effects are absolutely dominant in the non-equilibrium segregation because the non-equilibrium segregation levels of phosphorus predicted by the solute–interstitial complex model are much higher than those predicted by the solute–vacancy complex model. Moreover, for combined equilibrium and solute–interstitial complex-induced non-equilibrium segregation of phosphorus, the non-equilibrium segregation prevails below approximately 400°C and the equilibrium segregation dominates above this temperature.

Table 1
Data used in the theoretical calculations

Parameters	Phosphorus	Boron	Carbon
A_I	1	1	1
A_v	1	1	
E_f^v (eV)	1.4 [24]	1.4 [24]	
E_f^I (eV)	3.0	3.0	3.0
E_b^{iI} (eV)	0.57 [7]	1.11 [7]	1.12
E_b^{iv} (eV)	0.36 [7]	0.47 [7]	0.5
E_i (eV)	2.68 [3]	2.69 [25]	0.83 [25]
E_m^{iI} (eV)	0.87 [3]	1.41 [3]	1.42 [3]
E_m^{iv} (eV)	1.60 [26]	1.71 [26]	1.33
E_m^I (eV)	0.3 [27]	0.3 [27]	0.3 [27]
E_m^v (eV)	1.24 [8]	1.24 [8]	1.24 [8]
D_{oi} (m^2 s^{-1})	7.12×10^{-3} [3]	100 [25]	3.94×10^{-7} [25]
D_{oc}^{iv} (m^2 s^{-1})	1.7×10^{-5} [28]	1.7×10^{-5} [28]	3.94×10^{-7}
D_{oc}^{iI} (m^2 s^{-1})	8×10^{-7} [11]	8×10^{-7} [11]	8×10^{-7} [11]
D_{oI} (m^2 s^{-1})	5×10^{-6} [11]	5×10^{-6} [11]	5×10^{-6} [11]
D_{ov} (m^2 s^{-1})	5×10^{-5} [29]	5×10^{-5} [29]	5×10^{-5} [29]
Z_I	1.1 [30]	1.1 [30]	1.1 [30]
E_d (eV)	0.1 [31]	0.1 [31]	0.1 [31]
C_g (at.%)	0.072	0.0010	0.0010
B	0.01 [32,33]	0.01 [32,33]	0.01 [32,33]
b (m)	1.43×10^{-10}	1.43×10^{-10}	1.43×10^{-10}
β	0.775 [34]	0.775 [34]	0.775 [34]
Q (eV)	0.54 [35]	1.038 [36,37]	0.829 [38,39]
d (m)	1×10^{-9}	1×10^{-9}	1×10^{-9}

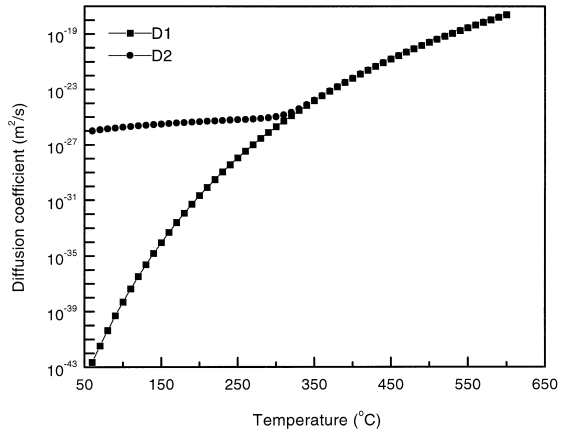

Fig. 1. The temperature dependence of phosphorus diffusion coefficient in the α-Fe matrix for thermal diffusion (D1) and irradiation-enhanced diffusion (D2), at a dose rate of 10^{-8} dpa s^{-1}, a dislocation density constant (ρ_o) of 10^{16} m^{-2}, and a grain size of 10 μm.

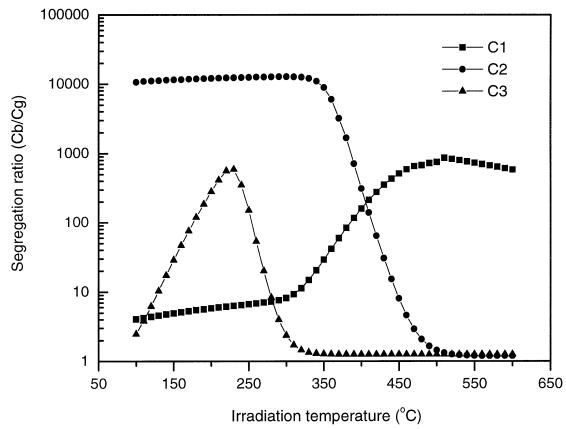

Fig. 2. The temperature dependence of equilibrium (C1) and non-equilibrium (predicted by the solute–interstitial complex (C2) and solute–vacancy complex (C3) models) phosphorus grain boundary segregation degree in α-Fe subjected to neutron irradiation ($\rho_o = 10^{16}$ m^{-2}, $R = 10$ μm, dose rate $= 10^{-8}$ dpa s^{-1}, dose $= 1$ dpa).

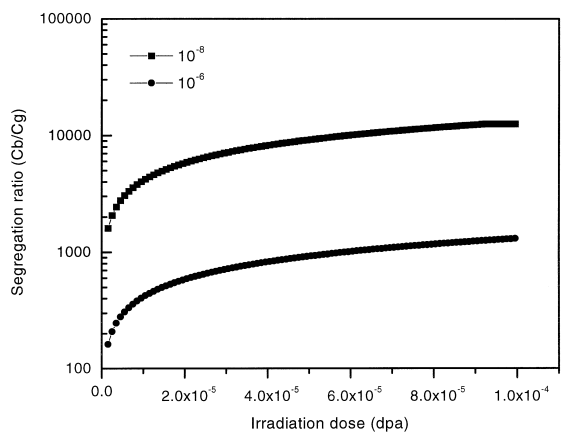

Fig. 3. The dose dependence of combined equilibrium and non-equilibrium phosphorus grain boundary segregation degree in α-Fe at 250°C for different dose rates (dpa s^{-1}), predicted by the solute–interstitial complex model ($\rho_o = 10^{16}$ m^{-2} and $R = 10$ μm).

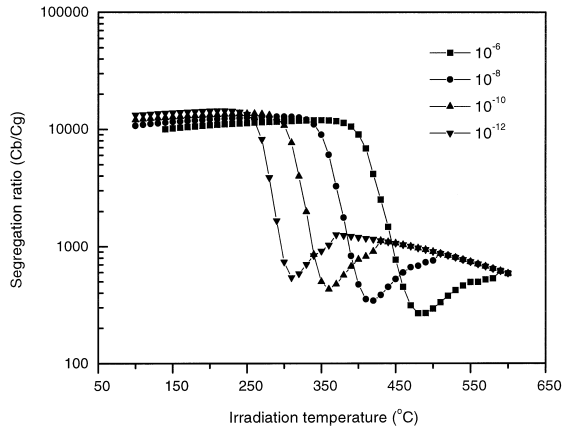

Fig. 4. The temperature dependence of combined equilibrium and non-equilibrium phosphorus grain boundary segregation degree in neutron-irradiated α-Fe at different dose rates (dpa s^{-1}), predicted by the solute–interstitial complex model ($\rho_o = 10^{16}$ m^{-2}, $R = 10$ μm, and dose = 1 dpa).

All the results shown in Figs. 3–8 are predicted by the solute–interstitial complex model. The segregation degree of phosphorus in α-Fe at 250°C is represented in Fig. 3 as a function of irradiation dose for different dose rates. Clearly, the segregation level increases with increasing irradiation dose until the steady-state segregation is achieved. The dose level required to reach the steady-state decreases with decreasing dose rate, because at the same dose level, the lower the dose

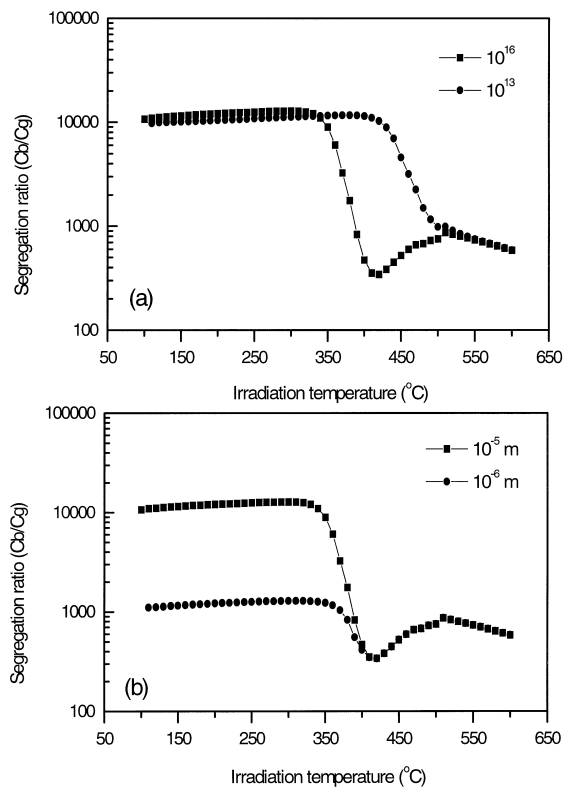

Fig. 5. The effects of (a) dislocation density constant (ρ_o, m^{-2}) and (b) grain size (R) on the combined equilibrium and non-equilibrium phosphorus grain boundary segregation degree in neutron-irradiated α-Fe, predicted by the solute–interstitial complex model (dose rate = 10^{-8} dpa s^{-1} and dose = 1 dpa; $R = 10$ μm for (a) and $\rho_o = 10^{16}$ m^{-2} for (b)).

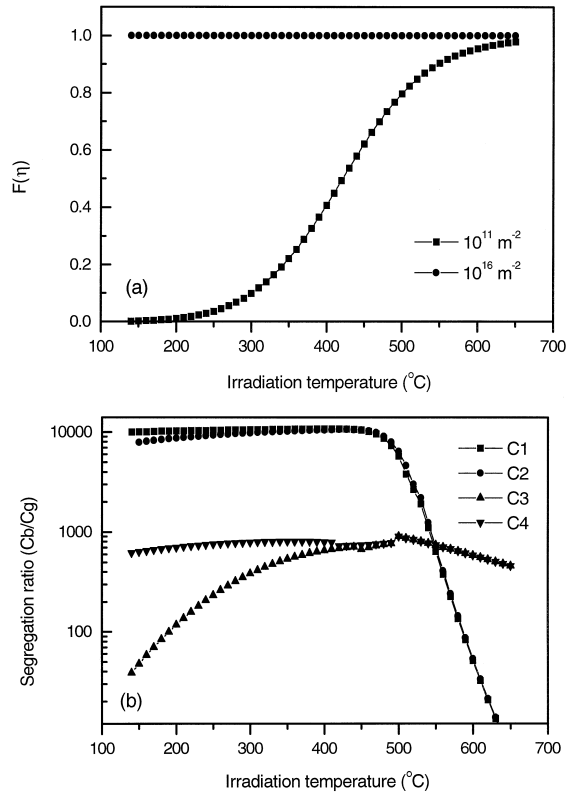

Fig. 6. (a) The long-range point-defect recombination term $F(\eta)$ as a function of irradiation temperature for different dislocation density constants. (b) The temperature dependences of non-equilibrium (C1 and C2) and equilibrium (C3 and C4) phosphorus grain boundary segregation in neutron irradiated α-Fe, predicted by the solute–interstitial complex model with (C1 and C3) and without (C2 and C4) consideration of the long-range point-defect recombination effect at a dislocation density constant of 10^{11} m^{-2} ($R = 10$ μm, dose rate $= 10^{-8}$ dpa s^{-1}, dose $= 1$ dpa).

rate, the longer is the time for segregation. Fig. 4 illustrates the effects of neutron dose rate in the range of 10^{-6} to 10^{-12} dpa s^{-1} on the combined segregation. Evidently, the phosphorus segregation peaks all shift to lower temperatures with decreasing neutron dose rate. The influences of dislocation density or grain size on the combined segregation are shown in Fig. 5a and b, respectively. Clearly, the dislocation density and the grain size both have an apparent effect on the phosphorus segregation during neutron irradiation. As discussed in Ref. [3], the influence of dislocation density is reflected in the kinetics of equilibrium segregation and in the quasi-thermodynamics of irradiation-induced non-equilibrium segregation, and that of grain size is brought about mainly by its influence on the critical time t_c.

In order to reveal the effect of the long-range recombination of freely migrating point-defects on segregation, we have, as illustrated in Fig. 6a, calculated the long-range recombination term $F(\eta)$ as a function of irradiation temperature for different dislocation density constants which characterise the sink strength. Clearly, there is no apparent long-range point-defect recombination effect for a dislocation density constant of 10^{16} m^{-2} (see Fig. 6a). This is because, as discussed in Ref. [40], the sink strength is so strong within the grain that the long-range recombination effect of freely migrating point-defects is negligible. When the dislocation density constant is reduced to 10^{11} m^{-2}, there emerges a noticeable long-range point-defect recombination effect (see Fig. 6a). Fig. 6b represents the temperature dependences of irradiation-induced non-equilibrium segregation (C1 and C2) and equilibrium segregation (C3 and C4) of phosphorus in neutron-irradiated α-Fe, with (C1 and C3) and without (C2 and C4) consideration of the long-range point-defect recombination effect at a dislocation density constant of 10^{11} m^{-2}. Clearly, the long-range point-defect recombination exerts some effect on both the non-equilibrium segregation and the equilibrium segregation. For the non-equilibrium segregation, the segregation level including the $F(\eta)$ effect is somewhat higher than that without considering the $F(\eta)$ effect at low temperatures, but it is slightly lower at higher temperatures. This phenomenon may be explained by the following considerations. On the one hand, the irradiation-enhanced phosphorus diffusivity decreases with decreasing $F(\eta)$, leading to an increase in the critical time (see Eqs. (5), (14) and (21)) and thus an increase in the non-equilibrium segregation. On the other hand, the maximum

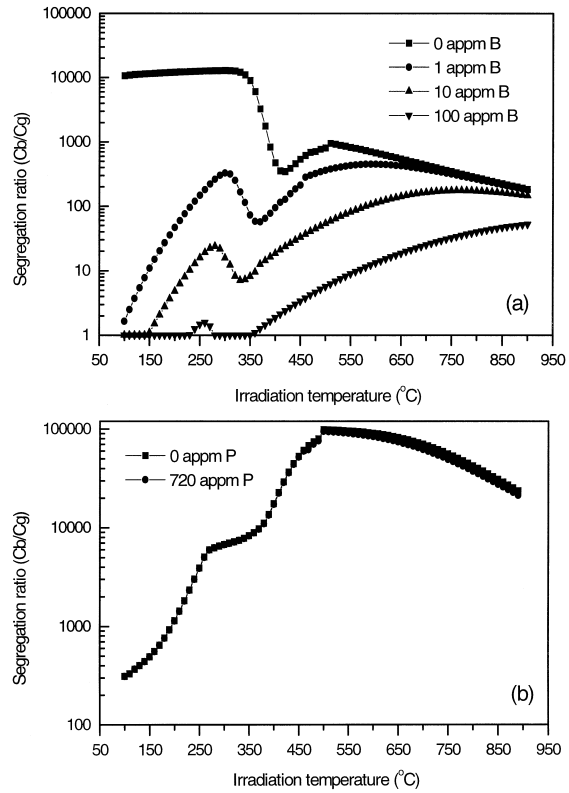

Fig. 7. The grain boundary segregation degree during neutron irradiation of (a) phosphorus in Fe: 0.072 at.% P–B (0, 1, 10, and 100 appm B) alloy, and of (b) boron in Fe: 0.0010 at.% B–P (0 and 720 appm P) alloy as a function of irradiation temperature, predicted by the site competition model ($\rho_o = 10^{16}$ m^{-2}, $R = 10$ μm, dose rate $= 10^{-8}$ dpa s^{-1}, dose $= 1$ dpa).

non-equilibrium segregation decreases with decreasing $F(\eta)$ (see Eq. (9)). In other words, non-equilibrium segregation is affected in opposite ways, depending on whether the critical time is exceeded or not. In the present example, low temperatures cause such low irradiation-enhanced diffusion because of the low $F(\eta)$ that the critical time becomes much greater as compared to the situation where we have not included the $F(\eta)$ effect. The overall non-equilibrium segregation is, therefore, somewhat enhanced. At higher temperatures, the maximum non-equilibrium segregation reduction effect is dominating although the critical time is somewhat increased. For the equilibrium segregation, $F(\eta)$ influences the predicted segregation predominantly in the low temperature range because of the decreased irradiation-enhanced phosphorus diffusivity.

Grain boundary segregation of phosphorus during neutron irradiation in Fe–B–P alloy, predicted by the ternary site competition model for different free boron concentrations, is shown in Fig. 7a as a function of irradiation temperature. Because of competition for sites at grain boundaries between boron and phosphorus, phosphorus segregation is considerably suppressed, especially at lower temperatures. Boron segregation dominates during neutron irradiation and is slightly affected by the site competition of phosphorus with boron in the high-temperature range only (see Fig. 7b).

Grain boundary segregation of phosphorus during neutron irradiation in Fe–C–P alloy, predicted by the site competition model for different free carbon concentrations, is illustrated in Fig. 8a as a function of irradiation temperature. Akin to the solute segregation in Fe–B–P alloy, phosphorus segregation is suppressed, notably at lower temperatures, due to the competition of carbon with phosphorus for segregation sites. However, the extent of the suppression in this alloy is less than that in Fe–B–P alloy. Carbon segregation is dominant in this alloy and is somewhat influenced by the site competition of phosphorus with carbon in the high-temperature range (see Fig. 8b).

Note that there are some differences between the temperature dependences of carbon and boron grain boundary segregation. As illustrated in Fig. 7b and Fig. 8b, the segregation peak temperature of carbon in Fe–C–P alloy, as compared to that in Fe–B–P alloy, shifts to lower temperatures and, below 500°C, the segregation level of carbon is much higher than that of boron. This is because the activation energy for carbon diffusion is much lower than that for boron diffusion in ferritic steels.

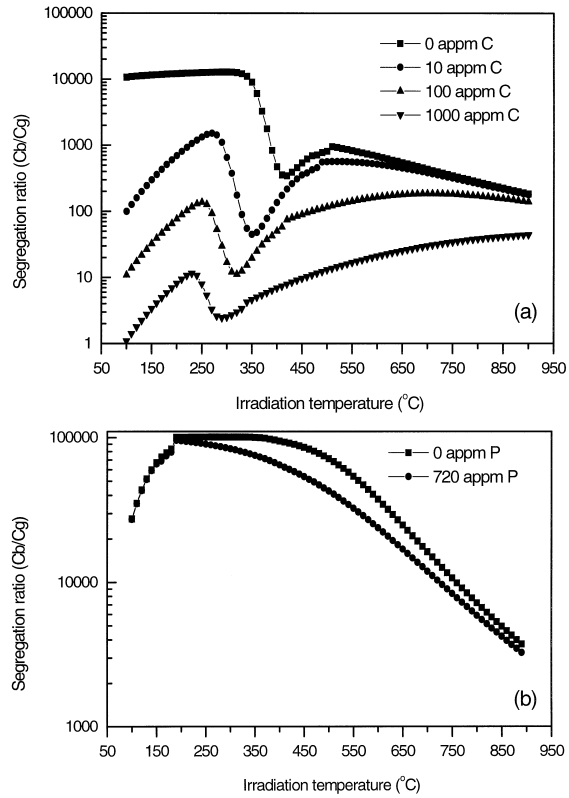

Fig. 8. The grain boundary segregation degree during neutron irradiation of (a) phosphorus in Fe: 0.072 at.% P–C (0, 10, 100, and 1000 appm C) alloy, and of (b) carbon in Fe: 0.0010 at.% C–P (0 and 720 appm P) alloy as a function of irradiation temperature, predicted by the site competition model ($\rho_o = 10^{16}$ m^{-2}, $R = 10$ μm, dose rate $= 10^{-8}$ dpa s^{-1}, dose $= 1$ dpa).

It may be concluded that since the ability to compete for segregation sites increases considerably on going from phosphorus to carbon to boron, grain boundary segregation of phosphorus during neutron irradiation in ferritic steels may be restrained, especially at lower temperatures, by minor boron or even carbon additions. Dissolved free carbon may restrain phosphorus segregation in ferritic steels. However, dissolved carbon content, in reality, is extremely low in commercial ferritic structural steels. Moreover, the competition ability of carbon is less than that of boron. Consequently, boron is more effective at suppressing phosphorus segregation when compared to carbon.

Until the present time, there have been quite limited experimental results on the phosphorus segregation during neutron irradiation in dilute binary alloys. Studies by Kameda and Bevolo [41] demonstrate that the grain boundary segregation level of phosphorus in a dilute Fe–P binary alloy is quite high and is much higher than that in a dilute Fe–C–P ternary alloy when they are both subjected to neutron irradiation to 9.4×10^{22} n m^{-2} (neutron energy > 0.1 MeV; ~ 0.005 dpa [8,42]) with a neutron flux of 2.1×10^{-17} n m^{-2} s^{-1} (neutron energy > 0.1 MeV; $\sim 1 \times 10^{-8}$ dpa s^{-1} [8,42]) at an irradiation temperature of 395°C. A 0.0073-wt% B-containing 10% Cr martensitic steel subjected to proton irradiation to 0.09 dpa with a dose rate of 9.4×10^{-7} dpa s^{-1} at 250°C exhibits that there is no phosphorus detected by FEGSTEM (field emission gun scanning transmission electron microscopy) microanalysis at grain boundaries. [1] Beere examined a series of C–Mn submerged-arc weld metals subjected to neutron irradiation in the range of 190–400°C. [2] His results demonstrate that the grain boundary segregation of phosphorus decreases with decreasing irradiation temperature. An investigation by Little et al. [43] on the microchemistry of neutron-irradiated 12% CrMoVNb martensitic steel showed an apparent phosphorus segregation to lath boundaries as the material was irradiated to 46 dpa at 465°C. A Loughborough study [44] was made in a 0.14-at.% P-doped 2.25 Cr1Mo steel, water-quenched, and irradiated to a neutron dose of ~ 0.042 dpa at a neutron dose rate of $\sim 1.05 \times 10^{-8}$ dpa s^{-1} (neutron energy > 1 MeV) at temperatures around 270°C (see curve C1 in Fig. 9) in a thermal,

[1] P. Marmy, EPFL-CRPP, Fusion Technology, CH-5232 Villigen PSI, Switzerland, private communication, 1996.
[2] W. Beere, Berkeley Centre, Magnox Electric, Berkeley, Gloucestershire, UK, private communication, 1996.

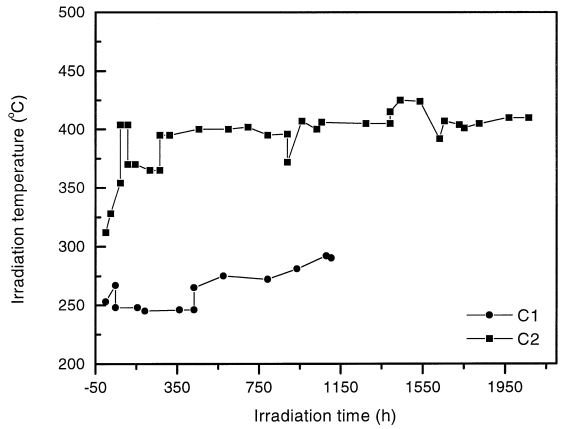

Fig. 9. Irradiation temperature as a function of irradiation time used in Ref. [44] ([3]).

light–water research reactor, named SAPHIR, operated by the Swiss Federal Institute for Reactor Research (the quenching-induced phosphorus grain boundary segregation is ~ 3.8 at.% [26]). FEGSTEM microanalysis of the grain boundary demonstrates that there is only ~ 0.2 at.% P grain boundary segregation during irradiation (the total segregation is ~ 4 at.%). However, the same material subjected to neutron irradiation to a dose of ~ 0.13 dpa with a neutron dose rate of $\sim 1.75 \times 10^{-8}$ dpa s^{-1} (neutron energy > 1 MeV) at temperatures around 400°C (see curve C2 in Fig. 9) exhibits ~ 3.2 at.% P grain boundary segregation during irradiation (the total segregation is ~ 7 at.%). [3]

A comparison of the predicted results from the ternary site competition model with some experimental values from Ref. [44] on the phosphorus segregation is indicated in Fig. 10 ([3]). The predictions are made for different free carbon contents and with the following irradiation conditions: (a) neutron dose rate $= 1.75 \times 10^{-8}$ dpa s^{-1} and neutron dose $= 0.13$ dpa; and (b) neutron dose rate $= 1.05 \times 10^{-8}$ dpa s^{-1} and neutron dose $= 0.042$ dpa. The experimental data points for the 0.14 at.% P-doped 2.25 Cr1Mo steel described above are plotted at 400 and 270°C, respectively, because, as shown in Fig. 9, the appropriate irradiation temperatures for comparison between the predicted and experimental results are about 400 and 270°C, respectively. Because of competition for sites at grain boundaries between carbon and phosphorus, phosphorus segregation is considerably suppressed, especially at lower temperatures. Also, it is clear that there is quite a reasonable fit between the predictions and the observations when an appropriate free carbon content is employed in the calculations. For irradiation around 270°C, when the free carbon concentration is about 0.1 at.%, the predicted result is reasonably consistent with the experimental value. This free carbon concentration is close to the bulk concentration of carbon of 0.4 at.% in the experimental steel. For irradiation around 400°C, however, the free carbon concentration, at which the predicted result is in reasonable agreement with the experimental value, is about 0.01 at.%. This carbon concentration is far away from the bulk concentration of carbon in the experimental steel (0.4 at.%). These phenomena are reasonable because when the steel is aged around 270°C, only a very small amount of carbide precipitation may occur, leading to the free carbon content to be close to the bulk content, but when the steel is aged around 400°C, a large amount of carbide precipitation may take place, leading to a free carbon content well below the bulk content. A recent experimental study by Beere [45] on the correlation between phosphorus and carbon segregation has indicated that the phosphorus segregation decreases with increasing carbon segregation. It should be recognised that the steel is not a pure dilute ternary alloy. However, bearing in mind many thermal grain boundary segregation studies confirming the site competition effect between phosphorus and carbon or boron [46–51], we have assumed here that, except for phosphorus and carbon or boron, the steel matrix may be regarded as the host component in the dilute ternary alloy for modelling simplicity.

Using both the Murphy–Perks rate theory model [52] and the McLean [15] equilibrium segregation model, Druce et al. [53] predicted grain boundary segregation of phosphorus in ferritic C–Mn submerged-arc weld metal subjected to neutron irradiation. Comparison of the present results with those calculated by Druce et al. [53] is represented in Fig. 11. Clearly, each of these two predictions forecasts the trends of segregation in the same way. Site competition and microstructural effects are not considered however in the rate theory model [53].

[3] R.G. Faulkner, S.-H. Song, P.E.J. Flewitt, Loughborough University, Leicestershire, UK, unpublished research, 1996.

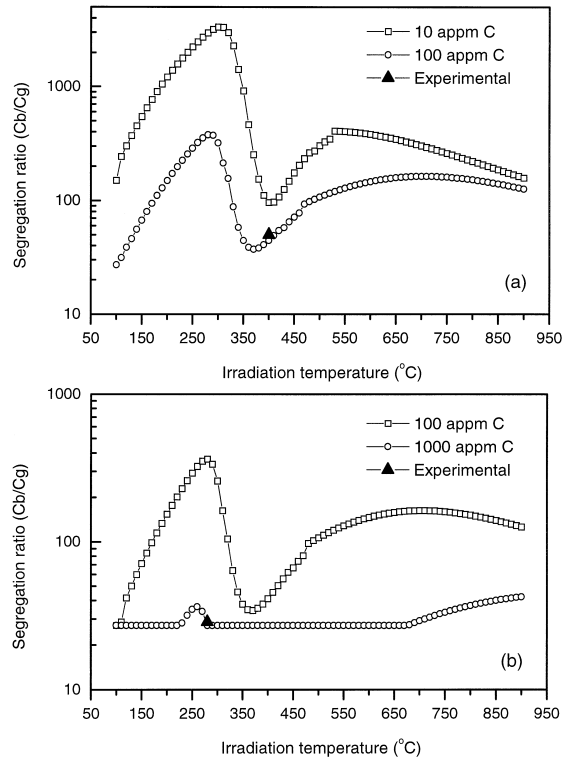

Fig. 10. The grain boundary segregation degree of phosphorus during neutron irradiation in Fe–C-0.14 at.% P alloys as a function of irradiation temperature, predicted for different free carbon concentrations and with irradiation conditions: (a) dose rate = 1.75×10^{-8} dpa s^{-1} and dose = 0.13 dpa; and (b) dose rate = 1.05×10^{-8} dpa s^{-1} and dose = 0.042 dpa. The experimental mean value is plotted for comparison (grain size = 10 μm and dislocation density constant = 10^{15} m^{-2}, and pre-irradiation boundary concentration = 3.8 at.%).

In order to compare with the Johnson–Lam rate theory model [11], we have predicted, using the interstitial–solute complex mechanism, irradiation-induced non-equilibrium zinc segregation at the thin foil surface of an Ag–Zn alloy and compared, as illustrated in Fig. 12, with those predicted by Johnson and Lam [11]. It may be seen evidently that these two predictions are consistent with each other in the trend of segregation.

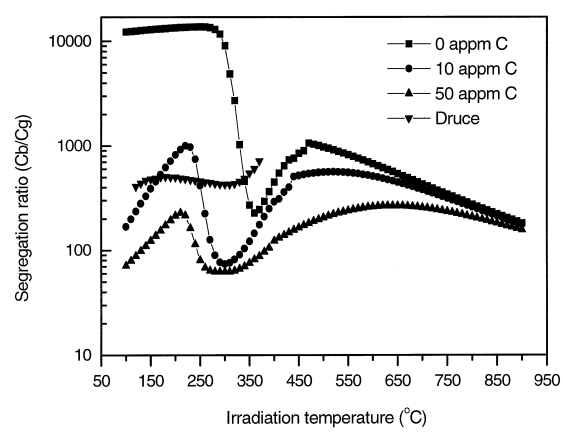

Fig. 11. The temperature dependence of combined equilibrium and non-equilibrium phosphorus grain boundary segregation degree for different free carbon concentrations in Fe–C–P alloy with the Druce results [53] for ferritic C–Mn submerged-arc weld metal plotted for comparison ($\rho_o = 10^{15}$ m^{-2}, $R = 10$ μm, dose rate = 5×10^{-12} dpa s^{-1}, dose = 0.005 dpa, phosphorus matrix concentration = 0.072 at.%, pre-irradiation phosphorus boundary concentration = 4.5 at.%).

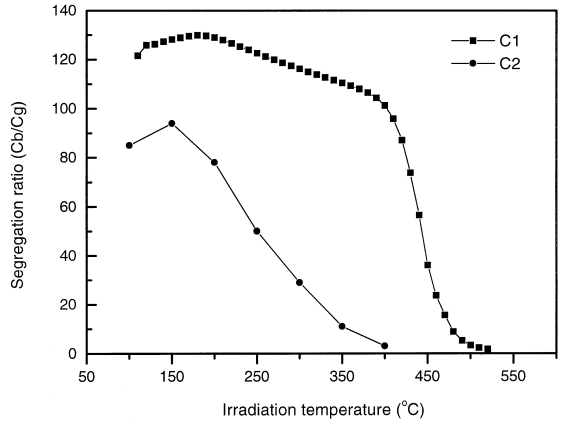

Fig. 12. The temperature dependence of irradiation-induced non-equilibrium zinc segregation at the thin foil surface of an Ag–Zn alloy (C1) with the Johnson–Lam results [11] plotted for comparison (C2) (parameters used in the calculation: $R = 0.1$ μm, $\rho_o = 10^{15}$ m^{-2}, dose rate $= 10^{-6}$ dpa s^{-1}, irradiation time $= 4$ days, $E_i = 1.53$ eV, $D_{oi} = 4.6\times10^{-5}$ m^2 s^{-1}, $E_m^I = 0.1$ eV, $D_{oI} = 5\times10^{-6}$ m^2 s^{-1}, $E_m^v = 0.84$ eV, $D_{ov} = 5\times10^{-5}$ m^2 s^{-1}, $E_m^{iI} = 0.3$ eV, $D_{oc} = 8\times10^{-7}$ m^2 s^{-1} $E_b^{iI} = 0.2$ eV, $E_f^v = 1.0$ eV, $b = 2.89\times10^{-10}$ m; other data used are listed in Table 1 (column 2)).

As stated earlier, a steady-state analytical solution of the Johnson–Lam rate theory model [11] has been derived by Martin [10]. This solution may be expressed as

$$C_b = C_g\left(\frac{a_v}{a_I}\right)^{-\tau}\left[\left(1+\frac{a_v}{a_I}\right)\left(\frac{C_v^r + C_v^e}{C_v^e}\right) - 1\right]^{\tau}, \tag{35}$$

where C_b is the steady-state solute concentration at the sink; C_g is the solute concentration in the matrix; a_I and a_v are the

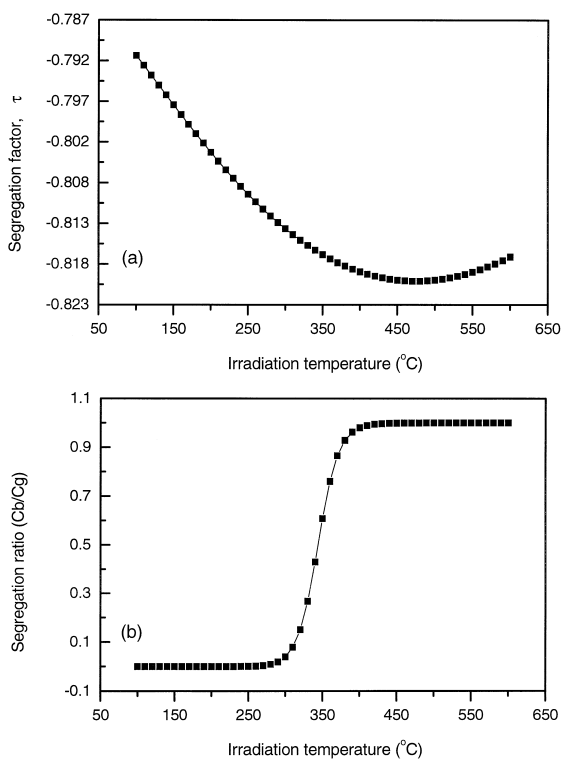

Fig. 13. (a) The segregation factor, τ, as a function of irradiation temperature. (b) The grain boundary segregation degree of phosphorus in neutron-irradiated α-Fe, predicted here by the steady-state analytical solution of the Johnson–Lam rate theory model.

positive functions of the jump frequencies of the respective defects in the vicinity of the solute; $\tau = (b_I + b_v)/(a_I + a_v)$, termed here the segregation factor, where b_I and b_v are the coupling parameters of the solute flux with the interstitial and vacancy fluxes, respectively. Determination of the parameters a_I, a_v, b_I, and b_v is given in Appendix A.

It may be seen from Eq. (35) that the segregation factor, τ, determines enrichment or depletion of solute atoms at sinks. The temperature dependence of segregation factor τ is illustrated in Fig. 13a for phosphorus in α-Fe. Clearly, τ is negative over the temperature range concerned. This means that phosphorus is depleted at sinks, especially at lower temperatures because of larger supersaturation degrees of point-defects, which is shown in Fig. 13b. These predicted results appear to be unreasonable because the present predictions (see Figs. 2–6) and many experimental studies [41,43–45,53,54] have demonstrated that there is apparent phosphorus grain boundary segregation under neutron irradiation in ferritic steels ([2,3]). The reason for this phenomenon may be that the data used in the calculation are not quite appropriate to this steady-state analytical solution.

4. Summary

An earlier model describing solute segregation during neutron irradiation in dilute binary alloys is improved in terms of the irradiation-enhanced solute diffusion theory and the evaluation of the long-range recombination of freely migrating point-defects, and expanded to make predictions of solute segregation in dilute ternary alloys through consideration of solute–solute competition for segregation sites. In the absence of solute–interstitial interactions, solute segregation to sinks may occur via solute–vacancy complexes if the solute–vacancy binding energy is high enough. However, it should be remembered that the migration of solute–vacancy complexes is quite slow as compared to that of solute–interstitial complexes. Predictions of phosphorus grain boundary segregation in neutron irradiated α-Fe and Fe–B–P and Fe–C–P alloys have been made by means of the newly modified model, assuming the presence of each defect type separately in order to clearly indicate whether the solute–interstitial complex effect or the solute–vacancy complex effect dominates during neutron irradiation-induced segregation. The predicted results clearly show that it is reasonable to consider the phosphorus–interstitial complex effect to be dominant during phosphorus segregation caused by neutron irradiation in ferritic steels. The site competition between phosphorus and boron or carbon may need to be taken into consideration for phosphorus segregation in the steels because both boron and carbon are predicted to suppress dramatically the segregation of phosphorus. Comparison of the model predictions with existing experimental results demonstrates that there is a reasonable agreement between the predictions and the observations.

5. List of symbols

a	Lattice constant of the matrix material
A_p	Constant related to the vibrational entropy of atoms around the point-defect (vacancy, v, or interstitial, I)
b	Jump distance of interstitials
B	Dose rate correction factor, i.e., the fraction of freely migrating point-defects escaping from the cascade
$C_{bq}(t)$	Equilibrium segregation level as a function of irradiation time t at a given temperature
$C_{br}(t)$	Irradiation-induced non-equilibrium segregation level as a function of irradiation time t at a given temperature
C_{br}^m	Maximum concentration of irradiation-induced segregation at a given temperature
C_g	Solute concentration in the matrix
C_I^r	Irradiation-generated interstitial concentration
C_p^r	Concentration of irradiation-generated point-defects (vacancies or interstitials)
C_v^e	Equilibrium vacancy concentration
C_v^r	Irradiation-generated vacancy concentration
$C_\infty(T)$	Maximum equilibrium segregation level at temperature T
d	Grain boundary enriched thickness
D_c^{ip}	Diffusion coefficient of solute–point-defect complexes in the matrix (D_c^{iv} for solute–vacancy complex diffusion and D_c^{iI} for solute–interstitial complex diffusion)
D_i^T	Thermal diffusion coefficient of solute atoms in the matrix
D_i^*	Irradiation-enhanced diffusion coefficient of solute atoms in the matrix
D_p	Diffusion coefficient of point-defects in the matrix (D_v for vacancies and D_I for interstitials)

D_{oc}^{ip}	Pre-exponential constant for complex diffusion (D_{oc}^{iI} for solute–interstitial complex diffusion and D_{oc}^{iv} for solute–vacancy complex diffusion)
D_{oi}	Pre-exponential constant for diffusion of solute atoms
D_{op}	Pre-exponential constant for diffusion of point-defects (D_{oI} for interstitials and D_{ov} for vacancies
E_b^{ip}	Solute–point-defect binding energy (E_b^{iI} for the solute–interstitial complex and E_b^{iv} for the solute–vacancy complex)
E_d	Activation energy for dislocation recovery
E_f^p	Point-defect formation energy (E_f^I for the interstitial and E_f^v for the vacancy)
E_i	Activation energy for solute diffusion in the matrix
E_m^{ip}	Migration energy of complexes (E_m^{iI} for solute–interstitial complexes and E_m^{iv} for solute–vacancy complexes)
E_m^p	Migration energy of point-defects (E_m^I for interstitials and E_m^v for vacancies)
G	Point-defect production rate, i.e., neutron dose rate
k	Boltzmann's constant
k_{dp}^2	Sink strength for the point-defect (k_{dv}^2 for vacancies and k_{dI}^2 for interstitials)
Q	Equilibrium segregation energy
r_i	Solute atom radius
r_o	Matrix atom radius
r_s	Octahedral interstitial radius
R	Grain size
t	Time
t_c	Critical time
T	Absolute temperature
x	Distance
Z_I	Bias parameter defining the preferential interaction between interstitials and dislocations compared with that between vacancies and dislocations
α_n	Maximum non-equilibrium enrichment ratio
α_e	Maximum equilibrium enrichment ratio
β	Constant showing the vibrational entropy of the grain boundary region
δ	Numerical constant, also known as the critical time constant
λ	Long-range recombination coefficient of freely migrating point-defects
ρ	Dislocation density
ρ_o	Dislocation density constant

Acknowledgements

This work was supported by the Magnox Electric and is published with the permission of the Director of Technology and Central Engineering of Magnox Electric. Also, the authors would like to thank Dr. R.K. Wild of the University of Bristol for commenting on the manuscript. Last but not least, we are grateful to Mr. Duncan Meade of Loughborough University for helping in computing.

Appendix A. Determination of parameters a_I, a_v, b_I, and b_v

We now determine the parameters a_I, a_v, b_I, and b_v in Eq. (35). According to Martin [10] and Barbu and Lidiard [55], a_I, a_v, b_I, and b_v may be given for bcc crystals by

$$a_I = \frac{1}{3a^2 w_0^I} \exp\left(\frac{E_b^{iI}}{kT}\right) \lambda_{BB} \tag{A1}$$

$$a_v = \frac{7 w_2^v w_4^v}{w_0^v (2 w_2^v + 7 w_3^v)} \tag{A2}$$

$$b_{\mathrm{I}} = \frac{1}{3a^2 w_0^{\mathrm{I}}} \exp\left(\frac{E_{\mathrm{b}}^{\mathrm{iI}}}{kT}\right)\left(\lambda_{\mathrm{AB}} + \lambda_{\mathrm{BB}}\right) \tag{A3}$$

$$b_{\mathrm{v}} = -\frac{9 w_2^{\mathrm{v}} w_4^{\mathrm{v}}}{w_0^{\mathrm{v}}\left(2w_2^{\mathrm{v}} + 7w_3^{\mathrm{v}}\right)} \tag{A4}$$

in which

$$\lambda_{\mathrm{AB}} = \frac{12a^2 w_1^{\mathrm{I}} w_2^{\mathrm{I}}}{5w_1^{\mathrm{I}} + 3w_2^{\mathrm{I}} + w_{\mathrm{R}}^{\mathrm{I}}} \tag{A5}$$

$$\lambda_{\mathrm{BB}} = 3a^2 w_1^{\mathrm{I}}\left(\frac{w_1^{\mathrm{I}} + 3w_2^{\mathrm{I}} + w_{\mathrm{R}}^{\mathrm{I}}}{5w_1^{\mathrm{I}} + 3w_2^{\mathrm{I}} + w_{\mathrm{R}}^{\mathrm{I}}}\right), \tag{A6}$$

where a is the lattice constant of the matrix material; $E_{\mathrm{b}}^{\mathrm{iI}}$ is the solute–interstitial binding energy; w_n^{I} ($n = 0,1,2$, and R) is the jump frequency of interstitials (subscript 0 denotes the jump leading to migration of the self-interstitial; subscript 1, leading to migration of the mixed dumbbell (solute–interstitial complex); subscript 2, leading to dissociation of the mixed dumbbell; and subscript R, leading to rotation of the interstitial dumbbell without a migration step onto a different lattice site); w_n^{v} ($n = 0$, 2, 3, and 4) is the jump frequency of vacancies (subscript 0 denotes the jump leading to migration of vacancies; subscript 2, leading to solute–vacancy interchange; subscript 3, leading to dissociation of the solute–vacancy complex; subscript 4, leading to formation of the solute–vacancy complex).

The various jump frequencies of interstitials and vacancies are given by [52]

$$w_{\mathrm{n}}^{\mathrm{I}} = 5 \times 10^{12} \exp\left(-\frac{E_{\mathrm{n}}^{\mathrm{I}}}{kT}\right), \qquad n = 0, 1, 2, \text{ and R} \tag{A7}$$

$$w_{\mathrm{n}}^{\mathrm{v}} = 5 \times 10^{13} \exp\left(-\frac{E_{\mathrm{n}}^{\mathrm{v}}}{kT}\right), \qquad n = 0, 2, 3, \text{ and } 4, \tag{A8}$$

where $E_{\mathrm{o}}^{\mathrm{I}} = E_{\mathrm{M}}^{\mathrm{I}}$; $E_1^{\mathrm{I}} = E_{\mathrm{m}}^{\mathrm{iI}}$; $E_2^{\mathrm{I}} = E_{\mathrm{m}}^{\mathrm{I}} + E_{\mathrm{b}}^{\mathrm{iI}}$; $E_{\mathrm{R}}^{\mathrm{I}} = 0.75$ eV [52]; $E_{\mathrm{o}}^{\mathrm{v}} = E_{\mathrm{m}}^{\mathrm{v}}$; E_2^{v} = solute–vacancy interchange energy; $E_3^{\mathrm{v}} = E_{\mathrm{m}}^{\mathrm{v}} + E_{\mathrm{b}}^{\mathrm{iv}}$ and $E_4^{\mathrm{v}} = E_{\mathrm{m}}^{\mathrm{v}}$; (assumed here that there is no interaction between vacancies and matrix atoms). $E_{\mathrm{m}}^{\mathrm{I}}$, $E_{\mathrm{m}}^{\mathrm{iI}}$, $E_{\mathrm{b}}^{\mathrm{iI}}$, $E_{\mathrm{m}}^{\mathrm{v}}$, and $E_{\mathrm{b}}^{\mathrm{iv}}$ are given in Table 1. In the calculations, the solute–vacancy interchange energy is acquired by the difference between the solute diffusion activation energy and the vacancy formation energy.

References

[1] P.R. Okamoto, L.E. Rehn, J. Nucl. Mater. 83 (1979) 2.
[2] R.G. Faulkner, N.C. Waite, E.A. Little, T.S. Morgan, Mater. Sci. Eng. A 171 (1993) 241.
[3] R.G. Faulkner, S.-H. Song, P.E.J. Flewitt, Met. Mater. Trans. 27A (1996) 3381.
[4] P.H. Dederichs, C. Lehman, H.R. Schober, A. Scholz, R. Zeller, J. Nucl. Mater. 69–70 (1978) 176.
[5] M.L. Swanson, L.M. Howe, J. Nucl. Mater. 69–70 (1978) 372.
[6] L.E. Rehn, K.-H. Robrock, H. Jacques, J. Phys. F 8 (1978) 1835.
[7] R.G. Faulkner, S.-H. Song, P.E.J. Flewitt, Mater. Sci. Technol. 12 (1996) 904.
[8] L.K. Mansur, Mechanisms and kinetics of radiation effects in metals and alloys, in: G.R. Freeman (Ed.), Kinetics of Non-homogeneous Processes, Wiley, New York, 1987, pp. 377–463.
[9] G.V. Kidson, J. Nucl. Mater. 118 (1983) 115.
[10] G. Martin, Philos. Mag. A 38 (1978) 131.
[11] R.A. Johnson, N.Q. Lam, Phys. Rev. B 13 (1976) 4364.
[12] R.G. Faulkner, J. Mater. Sci. 16 (1981) 373.
[13] S.-H. Song, T.-D. Xu, Z.-X. Yuan, Acta Metall. 37 (1989) 319.
[14] P. Shewmon, Diffusion in Solids, 2nd edn., Minerals, Metals and Materials Society, Warrendale, PA, 1989, pp. 53–130.
[15] D. McLean, Grain boundaries in metals, Oxford Univ. Press, London, 1957.
[16] M.P. Seah, Acta Metal. 25 (1977) 345.
[17] P.E. Busby, C. Wells, J. Met. 6 (1954) 972.
[18] C.C. McBride, J.W. Spretank, R. Speiser, Trans. Am. Soc. Met. 46 (1954) 499.
[19] F. Dworschak, R. Lennartz, H. Wollenberger, J. Phys. F 5 (1975) 400.
[20] F. Dworschak, Th. Monsau, H. Wollenberger, J. Phys. F 6 (1976) 2207.
[21] R.G. Faulkner, Mater. Sci. Technol. 1 (1985) 442.
[22] M.A.V. Chapman, R.G. Faulkner, Acta Metall. 31 (1983) 677.

[23] J.D.H. Donnay, H.M. Ondik (Eds.), Crystal Data—Determinative Tables, 3rd edn., Vol. 2, Published jointly by the US Department of Commerce, National Bureau of Standards and the Joint Committee on Powder Diffraction Standards, USA, 1973, pp. C1–C374.
[24] S.M. Kim, W.J.L. Buyers, J. Phys. F 8 (1978) L103.
[25] E.A. Brandes, G.B. Brook (Eds.), Smithells Metals Reference Book, 7th edn., Butterworth–Heinemann, Oxford, 1992, pp. 13-70–13-102.
[26] R.G. Faulkner, S.-H. Song, P.E.J. Flewitt, Mater. Sci. Technol. 12 (1996) 818.
[27] R.W. Cahn, P. Haasen (Eds.), Physical Metallurgy, 3rd edn., North-Holland, Amsterdam, 1983, p. 1189.
[28] S.-H. Song, R.G. Faulkner, Defect and Diffusion Forum 143–147 (1997) 149.
[29] T.M. Williams, A.M. Stoneham, D.R. Harries, Met. Sci. 10 (1976) 14.
[30] R. Bullough, M.R. Hayns, M.H. Wood, J. Nucl. Mater. 90 (1980) 44.
[31] D. Hull, D.J. Bacon, Introduction to Dislocations, 3rd edn., Pergamon, Oxford, 1984, p. 79.
[32] V. Naundorf, M.-P. Macht, H. Wollenberger, J. Nucl. Mater. 186 (1992) 227.
[33] H. Trinkaus, V. Naundorf, B.N. Singh, C.H. Woo, J. Nucl. Mater. 210 (1994) 244.
[34] T. Qgura, Trans. Jan. Inst. Met. 22 (1981) 109.
[35] Ph. Dumoulin, M. Guttmann, M. Foucault, M. Palmier, M. Wayman, M. Biscondi, Met. Sci. 14 (1980) 1.
[36] M. Hashimoto, Y. Ishida, R. Yamamoto, M. Doyama, Acta Metall. 32 (1984) 1.
[37] C.M. Liu, T. Nagoya, K. Abiko, H. Kimura, Met. Trans. 23A (1992) 263–269.
[38] E. Erhart, H.J. Grabke, Met. Sci. 15 (1981) 401–408.
[39] S. Suzuki, M. Obata, K. Abiko, H. Kimura, Scr. Metall. 17 (1983) 1325–1328.
[40] R. Sizmann, J. Nucl. Mater. 69–70 (1978) 386.
[41] J. Kameda, A.J. Bevolo, Acta Metall. 37 (1989) 3283.
[42] M.J. Norgett, M.T. Robinson, I.M. Torrens, Nucl. Eng. Des. 33 (1975) 50.
[43] E.A. Little, T.S. Morgan, R.G. Faulkner, Mater. Sci. Forum 97–99 (1992) 323.
[44] S.-H. Song, PhD Thesis, Loughborough University, Leicestershire, UK, 1995.
[45] W. Beere, Report No. TE/GEN/REP/0152/97, Issue 1, Berkeley Centre, Magnox Electric, Berkeley, Gloucestershire, UK, 1997.
[46] S. Suzuki, N. Obata, K. Abiko, H. Kimura, Scr. Metall. 17 (1983) 1325.
[47] S. Suzuki, N. Obata, K. Abiko, H. Kimura, Trans. ISIJ 25 (1985) 62.
[48] H. Erhart, H.J. Grabke, Met. Sci. 15 (1981) 401.
[49] C.M. Liu, T. Nagoya, K. Abiko, H. Kimura, Metall. Trans. 23A (1992) 263.
[50] T. Mega, J.-I. Shimomura, E. Yasuhara, Mater. Trans. JIM 36 (1995) 1206.
[51] T. Mega, J.-I. Shimomura, K. Seto, Mater. Trans. JIM 37 (1996) 323.
[52] S.M. Murphy, J.M. Perks, J. Nucl. Mater. 171 (1990) 360.
[53] S.G. Druce, C.A. English, A.J.E. Foreman, R.J. Mcelroy, I.A. Vatter, C.J. Bolton, J.T. Buswell, R.B. Jones, The modelling of irradiation-enhanced phosphorus segregation in neutron-irradiated RPV submerged-arc welds, in: D. Gelles, R.K. Nanstead, A.S. Kumar, E.A. Little (Eds.), Effects of Radiation on Materials, 17th International Symposium, ASTM STP 12XX, ASTM, Philadelphia, in press.
[54] T.S. Morgan, E.A. Little, R.G. Faulkner, J.M. Titchmarsh, in: R.E. Stoller, A.S. Kumar, D.S. Gelles (Eds.), Effects of Radiation on Materials, 15th Int. Symp., ASTM STP 1125, ASTM, Philadelphia, PA, 1992, pp. 633–644.
[55] A. Barbu, A.B. Lidiard, Philos. Mag. A 74 (1996) 709.